# Simple model to calculate surface magnetization from spin-polarized metastable deexcitation spectroscopy: Fe/Ag(100)

M. Salvietti,* R. Moroni, P. Ferro, M. Canepa, and L. Mattera†

*Unità Istituto Nazionale di Fisica della Materia (INFM) and Centro di Fisica delle Superficie Basse Temperature (CFSBT),
Dipartimento di Fisica, Università di Genova, via Dodecaneso 33, I-16146, Genova, Italy*

A simple model has been introduced to extract effective charge and magnetization densities at surface from spin-polarized metastable deexcitation spectroscopy data. The model has been applied to the case study of a 10-ML film of Fe deposited at $T = 120$ K on Ag(100). The charge and magnetization densities which have been calculated compare well with the experimental and theoretical data available on this system. In particular, the energy shift of 0.3 eV between the majority and the minority densities of states near the Fermi edge detected by spin-polarized photoemission is reproduced with high accuracy. [S0163-1829(96)03044-5]

## I. INTRODUCTION

The magnetic properties of surfaces and thin films have attracted a great amount of interest in the last few years both theoretically and experimentally.[1,2] A variety of phenomena determined by the low dimensionality of these systems is responsible for such interest. To mention a few, we may recall the interplay between crystallographic order and magnetic properties,[3] the influence of temperature and film thickness on the direction of magnetization,[4] the magnetic anisotropy,[5] and the influence of film purity as determined by diffusion and segregation from the substrate on the surface magnetization. Some of these phenomena are or may become technologically relevant.

Experimentally, a great variety of techniques have been employed to investigate surface and thin film magnetism.[1] Here we will deal with spin-polarized metastable deexcitation spectroscopy (SPMDS) which exploits the deexcitation at surface of a spin-polarized He atom in a metastable, excited electronic state to provide information on the surface magnetism.[6,7]

The deexcitation processes, extensively described in several papers in the case of unpolarized[8] and polarized[9] metastable atoms, ensure an extreme surface sensitivity which can be exploited to investigate phenomena typical of surfaces as the influence on magnetic properties of adsorbates or particles segregated at surface during the growth or following the preparation of the film. Furthermore, this sensitivity can be essential in the investigation of ultrathin films at the monolayer level.

A major limit of this spectroscopy, however, has always been the difficulty in extracting quantitative information from the experimental data, in particular when the deexcitation process occurs via the two steps mechanism of resonant ionization followed by Auger neutralization (RI+AN) typical of metal surfaces characterized by a *large* value ($\simeq 4$ eV) of the work function. In this category most of the metal surfaces and in particular the $3d$ magnetic ones are found.

In this case, the work function is higher then the He* ionization potential, so that the electron in the excited state of He* is degenerate in energy with one of the empty levels in the metal. As He* approaches the surface and the wave function of the excited electron overlaps the tail of the wave function of the empty states, the excited electron tunnels into the metal and a He$^+$ ion is formed (RI). This step occurs with almost unit probability at large distances from the surface ($z_{RI} \gtrsim 5$ Å).[9]

The ion is then accelerated toward the surface by the image potential, and neutralized by an Auger process (AN) where a conduction electron from the metal fills the $1s$ hole and a second electron is ejected from the surface. The surface specificity of this spectroscopy derives from the fact that this step is effective at a distance $z_{AN} \simeq 2-3$ Å out of the surface plane, and is then sensitive to the tail of the electron density of states spilling out into vacuum.

If the incoming He*($2\,^3S$) is spin polarized, the $1s$ hole of He$^+$ has a defined spin which has to be matched by the neutralizing electron. The neutralization step is then sensitive to the spin-selected density of states at the surface, and, reversing the spin polarization of the incoming atom, the two spin-selected density of states are sampled.

In particular, one can *measure* the surface magnetization by introducing the asymmetry

$$A^{\text{expt}}(E) = \frac{1}{P} \frac{I_\downarrow(E) - I_\uparrow(E)}{I_\downarrow(E) + I_\uparrow(E)} , \qquad (1.1)$$

where $P$ is the polarization degree of the He* beam impinging on the surface, and $I_{\downarrow(\uparrow)}(E)$ are the experimental energy distributions of the electrons ejected following the interaction of spin-polarized He* atoms with polarization parallel ($\uparrow$) or antiparallel ($\downarrow$) to the magnetization direction of the sample.

In this paper we will develop a simple model to extract quantitative information on the surface magnetization from the measured asymmetry. We will start from the theory developed by Penn and Apell[9] and employed to interpret SPMDS data on the Ni(110) surface.[7] The definitions and the major steps of the theory will be reported here for convenience, but the interested reader is referred to the original paper for a thorough discussion and all details.

The model will be presented in Sec. II, and applied to the case study of a 10-ML film of iron grown on Ag(100) at

$T = 120$ K. The apparatus and the experimental results on this system will be presented in Sec. III. The results of the model will be given in Sec. IV, and discussed in Sec. V. Finally, conclusions will be presented in Sec. VI.

## II. MODEL

As anticipated in Sec. I, the two steps occurring in the deexcitation process are effective at well-separated distances from the surface, so that they can be treated independently. Furthermore, the first step (RI) occurs with a practically unit probability and is independent of spin polarization.[9]

The study of the deexcitation process therefore reduces to the study of the Auger neutralization (AN step) of He$^+$ ions having a $1s$ hole with $\uparrow(\downarrow)$ spin (He$^+_{\uparrow(\downarrow)}$ hereafter). We start from the definition of the theoretical asymmetry as

$$A(E) = \frac{N_\downarrow(E) - N_\uparrow(E)}{N_\downarrow(E) + N_\uparrow(E)}, \qquad (2.1)$$

where $N_{\uparrow(\downarrow)}(E)$ represents the energy distribution of the electrons emitted from the sample following the neutralization of He$^+_{\uparrow(\downarrow)}$.

If $q_{\uparrow(\downarrow)}(z)$ is defined as the probability that He$^+_{\uparrow(\downarrow)}$ survives at a distance $z$ from the surface and $r_{\uparrow(\downarrow)}(E,z)$ as the probability per unit time that an electron is ejected with energy $E$ following the neutralization of He$^+_{\uparrow(\downarrow)}$ at a distance $z$, then

$$N_{\downarrow(\uparrow)}(E) = \int_0^\infty \frac{dz}{v(z)} r_{\downarrow(\uparrow)}(E,z) q_{\downarrow(\uparrow)}(z). \qquad (2.2)$$

In Eq. (2.2), $v(z) = -dz/dt$ is the ion velocity which can be calculated from

$$\frac{1}{2} M v^2(z) = E_{\text{inc}} + \frac{e^2}{4z}, \qquad (2.3)$$

where $M$ is the ion mass, $E_{\text{inc}}$ is the asymptotic kinetic energy, and $e^2/4z$ is the image potential sampled by the ion as it approaches the surface.

$q$ and $r$ are linked by the rate equation

$$\frac{dq_{\uparrow(\downarrow)}(z)}{dz} = \frac{R_{\uparrow(\downarrow)}(z) q_{\uparrow(\downarrow)}(z)}{v(z)}, \qquad (2.4)$$

where

$$R_{\uparrow(\downarrow)}(z) = \int_0^\infty dE \ r_{\uparrow(\downarrow)}(E,z) \qquad (2.5)$$

gives the probability per unit time that an electron is produced by an Auger process which neutralizes He$^+_{\uparrow(\downarrow)}$ at $z$.

Equation (2.4) admits the solution

$$q_{\uparrow(\downarrow)}(z) = \exp\left( -\int_z^\infty d\zeta \frac{R_{\uparrow(\downarrow)}(\zeta)}{v(\zeta)} \right), \qquad (2.6)$$

which allows us to calculate $q_{\uparrow(\downarrow)}(z)$ from the production rate $r_{\uparrow(\downarrow)}(E,z)$ of Auger electrons. In principle then, the knowledge of $r_{\uparrow(\downarrow)}(E,z)$ leads to $N_{\uparrow(\downarrow)}(E)$ and then to $A(E)$.

In order to calculate $A(E)$, Penn and Apell[9] conveniently expressed $q_{\uparrow(\downarrow)}(z)$ and $r_{\uparrow(\downarrow)}(E,z)$ as

$$q_\uparrow(z) = q_0(z) + \Delta q(z), \qquad (2.7)$$

$$q_\downarrow(z) = q_0(z) - \Delta q(z), \qquad (2.8)$$

$$r_\uparrow(E,z) = r_0(E,z) + \Delta r(E,z), \qquad (2.9)$$

$$r_\downarrow(E,z) = r_0(E,z) - \Delta r(E,z). \qquad (2.10)$$

The rates $R_0(z)$ and $\Delta R(z)$ can then be defined as

$$R_0(z) = \int_0^\infty dE \ r_0(E,z), \qquad (2.11)$$

$$\Delta R(z) = \int_0^\infty dE \ \Delta r(E,z), \qquad (2.12)$$

so that, to the lowest order in $\Delta R(z)$, we have

$$q_0(z) = \exp\left( -\int_z^\infty d\zeta \frac{R_0(\zeta)}{v(\zeta)} \right), \qquad (2.13)$$

$$\Delta q(z) = -q_0(z) \int_z^\infty d\zeta \frac{\Delta R(\zeta)}{v(\zeta)}. \qquad (2.14)$$

Insertion of Eqs. (2.7)–(2.14) in Eq. (2.1) allows us to expand $A(E)$ to the lowest order in $\Delta r$ and $\Delta q$, obtaining

$$A(E) = -\frac{\int_0^\infty \dfrac{dz}{v(z)} q_0(z) \left[ \Delta r(E,z) - r_0(E,z) \int_z^\infty d\zeta \dfrac{\Delta R(\zeta)}{v(\zeta)} \right]}{\int_0^\infty \dfrac{dz}{v(z)} q_0(z) r_0(E,z)}.$$

$$(2.15)$$

In the right-hand side of Eq. (2.15), the first term provides the contribution to the asymmetry of the unbalance $\Delta r$ of the rates $r_{\uparrow(\downarrow)}$, while the second term introduces a correction which takes into account the reduced availability of holes in He$^+_{\uparrow(\downarrow)}$ with the *right* spin determined by the rate unbalance. Equation (2.15) as well as all the definitions reported so far coincide with the results of Ref. 9.

Here, in order to simplify the calculation of $A(E)$, we assume that the neutralization of He$^+_{\uparrow(\downarrow)}$ occurs at a well defined distance $z_n$ from the surface so that, independently on the spin polarization of He$^+_{\uparrow(\downarrow)}$,

$$q_{\uparrow(\downarrow)}(z) = \begin{cases} 1, & z > z_n \\ 0, & z < z_n. \end{cases}$$

This assumption implies that $r_{\uparrow(\downarrow)}(E,z)$ and $R_{\uparrow(\downarrow)}(z)$ are different from zero only at $z = z_n$ and $\Delta R = 0$. The second term of Eq. (2.15) is then neglected, and the asymmetry can be simplified to

$$A(E) = -\frac{\Delta r(E,z_n)}{r_0(E,z_n)}. \qquad (2.16)$$

In order to determine $r_{\uparrow(\downarrow)}(E,z)$, following the approach of Penn and Apell,[9] the transition rates are calculated via the Fermi golden rule. They depend on the initial states of the

electron involved in the neutralization process $(l, \epsilon)$ and of the electron emitted from the sample $(l', \epsilon')$. Here $l, l'$ and $\epsilon, \epsilon'$ represent the orbital character and the energies of these states, respectively.

The matrix elements are assumed to be factorized in the product of two terms. The first can be identified with the wave function $\psi_{l, \epsilon}(z)$ of the metal electron which fills the $1s$ hole of He$^+$ (down electron), calculated at the ion position where the neutralization occurs. This term therefore, is determined by the decay into vacuum of the electron wave function, so that it depends strongly on the orbital character of the electron involved in the neutralization process. In particular, it can be expected that, due to the different localization, $s$-$p$ states do contribute more effectively then $d$ states.

The second term is assumed to depend on the orbital character of the occupied metal state $\Phi_{l', \epsilon'}(z)$ from where the Auger electron is created (up electron). Assuming that this term shows a small dependence on the position $z$ where neutralization takes place and on energy, it can be approximated as $\Phi_{l', \epsilon'}(z) \simeq \Phi_{l'}$.

Using these approximations and neglecting interference effects, we have

$$\Delta r(E, z) = \gamma \int d\epsilon \int d\epsilon' \, m_n(\epsilon, z) n_A(\epsilon')$$
$$\times \delta(\epsilon + \epsilon' - E - E_{1s}(z)), \quad (2.17)$$

$$r_0(E, z) = \gamma \int d\epsilon \int d\epsilon' \, n_n(\epsilon, z) n_A(\epsilon')$$
$$\times \delta(\epsilon + \epsilon' - E - E_{1s}(z)), \quad (2.18)$$

where

$$\gamma = \frac{\pi}{\hbar} \rho_s(E) \sum_l |\Phi_l|^2 \quad (2.19)$$

accounts for the availability of empty states of density $\rho_s(E)$ for the up electrons,

$$n_A(\epsilon) = \frac{\sum_l n_l(\epsilon) |\Phi_l|^2}{\sum_l |\Phi_l|^2} \quad (2.20)$$

provides the density of states from where emitted electrons originate, and

$$m_n(\epsilon, z) = \sum_l m_l(\epsilon) |\psi_{l, \epsilon}(z)|^2, \quad (2.21)$$

$$n_n(\epsilon, z) = \sum_l n_l(\epsilon) |\psi_{l, \epsilon}(z)|^2. \quad (2.22)$$

In Eqs. (2.20)–(2.22), $m_l(\epsilon) = \rho_{l, \uparrow} - \rho_{l, \downarrow}$ and $n_l(\epsilon) = \rho_{l, \uparrow} + \rho_{l, \downarrow}$ represent the magnetization and the charge density of surface localized orbitals of $l$ character, respectively.[9] $m_n(\epsilon, z)$ and $n_n(\epsilon, z)$ can then be interpreted as the magnetization and the charge densities effective in the neutralization process, i.e., as the magnetization and the charge sampled by the metastable atoms at the distance from the surface where the neutralization occurs weighted by the appropriate matrix elements.

The $\delta$ functions in Eqs. (2.17) and (2.18) account for energy conservation. In particular, $E_{1s}(z)$ is the ionization potential of the $1s$ level of He$^+$ at a distance $z$ from the surface plane. Due to the He$^+$-surface interaction, $E_{1s}(z)$ will be different from the asymptotic value $E_{1s}^\infty$ (isolated ion). $\epsilon = \epsilon_F + \phi$ and $\epsilon' = \epsilon_F' + \phi$ give the energy levels of the metal electrons involved in the process measured with respect to the vacuum level ($\epsilon_F$ and $\epsilon_F'$ are the corresponding quantities that refer to the Fermi level, and $\phi$ is the work function).

Insertion of Eqs. (2.17) and (2.18) into Eq. (2.16), with an appropriate change of variables, leads to

$$A(E) = -\frac{\int_0^\infty d\varepsilon \, m_n\left(\frac{E - E_{\max}}{2} - \varepsilon\right) n_A\left(\frac{E - E_{\max}}{2} + \varepsilon\right)}{\int_0^\infty d\varepsilon \, n_n\left(\frac{E - E_{\max}}{2} - \varepsilon\right) n_A\left(\frac{E - E_{\max}}{2} + \varepsilon\right)}, \quad (2.23)$$

where the explicit dependence on $z_n$ has been dropped and $E_{\max} = -(E_{1s}(z_n) + 2\phi)$ is the maximum kinetic energy of the emitted electrons ($\epsilon_F = \epsilon_F' = 0$, both electrons in the metal come from the Fermi level).

In this approximation, the asymmetry is expressed as the energy convolution of the effective magnetization at $z_n$, with the effective charge density, from which the emitted electron originates, normalized to the convolution of the charge densities from where the two electrons involved in the Auger process are created.

As introduced in Ref. 10 to calculate the electron energy distribution curves produced by unpolarized metastable atoms, a further simplification of Eq. (2.23) can be made by assuming that the two density of states involved in the AN step can be identified to an effective density of states $n(E)$, so that $n_n(E) = n_A(E) = n(E)$ and

$$A(E) = -\frac{\int_0^\infty d\varepsilon \, m\left(\frac{E - E_{\max}}{2} - \varepsilon\right) n\left(\frac{E - E_{\max}}{2} + \varepsilon\right)}{\int_0^\infty d\varepsilon \, n\left(\frac{E - E_{\max}}{2} - \varepsilon\right) n\left(\frac{E - E_{\max}}{2} + \varepsilon\right)}. \quad (2.24)$$

In Eq. (2.24), the suffix of $m_n(E)$ has been dropped for convenience and the denominator coincides with the energy spectrum $N(E)$ calculated by Sesselmann et al.[10] We can therefore start from guessed forms of $\rho_\uparrow(E)$ and $\rho_\downarrow(E)$, build $m(E) = \rho_\uparrow(E) - \rho_\downarrow(E)$ and $n(E) = \rho_\uparrow(E) + \rho_\downarrow(E)$, calculate the required convolutions and compare the results with the experimental asymmetry $A^{\text{expt}}(E)$ and the spectrum $I^{\text{expt}}(E)$.

## III. EXPERIMENT

The experimental details concerning the apparatus which employs SPMDS to study surface magnetism will be described elsewhere.[11] He* atoms are produced in a dc discharge between a tantalum tip and a stainless-steel skimmer through a nozzle in a quartz glass tube. The He* beam has an intensity on the sample of the order of $10^{11}$ at/s with a spot diameter of 1 mm.

In the beam, in addition to He atoms in the ground state, irrelevant in the present experiment, metastable atoms in the singlet and triplet states and UV photons are present. The populations of $He^*(2^1S)$ and photons are about 10% and 5% of $He^*(2^3S)$, respectively. Metastable atoms in the triplet state are spin polarized by optical pumping with 1.083-$\mu$m light supplied by a laser diode and circularly polarized by a quarter-wave plate. The effective polarization degree, including metastables in the singlet state, is 84% as obtained by a Stern-Gerlach analysis.[12] The energy spectra of the emitted electrons are taken in normal emission by a spectrometer characterized by an acceptance angle of about 0.4 sr, and an energy resolution of 250 meV.[13]

Iron is deposited on the silver substrate by electron bombardment of a rod. After a thorough outgassing of the iron source, the pressure in the scattering chamber remains below $2 \times 10^{-10}$ mbar during the whole operation of deposition.

The magnetization of the film is provided by a current pulse in a coil around the sample. A desired crystallographic direction of the sample can be set parallel to the axis of the coil by using the azimuthal rotation axis of the manipulator.

Measurements reported here were taken in remanence after in-plane magnetization of the iron film along the $\langle 100 \rangle$ direction, the easy magnetization axis of bcc iron. The atomic beam polarization is set parallel to the direction of magnetization of the sample by a quantization field of the order of 0.5 G, and it can be reversed by inverting the circular polarization of the laser beam after a 90° rotation of the quarter-wave plate.

In Fig. 1 the experimental results from a 10-ML Fe film deposited at $T = 120$ K on Ag(100) are reported. In the upper part of the figure, the energy distribution curves (EDC) of electrons produced in the deexcitation of $He^*_\uparrow$ [$I_\uparrow(E)$, upward pointing triangles] and of $He^*_\downarrow$ [$I_\downarrow(E)$, downward pointing triangles] are shown, while Fig. 1(b) shows the asymmetry $A^{expt}(E)$ [Eq. (1.1)]. We observe that the maximum of $A^{expt}(E)$ is of the order of 6%, well below the values obtained from SPMDS on Fe films grown on W(110) (Ref. 14) and GaAs.[15] This lower value of $A^{expt}(E)$ could be due to surface disorder, either crystallographic or compositional, of the Fe/Ag film. The disorder cannot be reduced by annealing the film, as the annealing induces the segregation of silver at the surface[16] with a degradation of $A^{expt}(E)$, a process which is active already at room temperature. The same effect is obtained by growing the film at higher temperatures of the substrate.[17]

In order to minimize the presence of Ag on the surface, we have then grown the film at low temperatures of the substrate without any annealing. This choice was supported by an ion backscattering analysis,[18] which shows that for a 10-ML film grown at $T = 135$ K, the fraction of silver on the surface is below 5%, consistent with the spectra of Fig. 1(a), where we do not observe significant contributions from the density of states of silver. [For a comparison between the EDC's from the Ag(100) substrate and the Fe film; see Fig. 1 of Ref. 17].

The rapid increase of the EDC right from $E_{max}$, shown in Fig. 1, denotes a high weight of the density of states near the Fermi edge consistently with the shape of the density of states of iron. In Fig. 1(b), we also notice the positive sign of $A^{expt}(E)$ with a small negative contribution far from $E_{max}$,
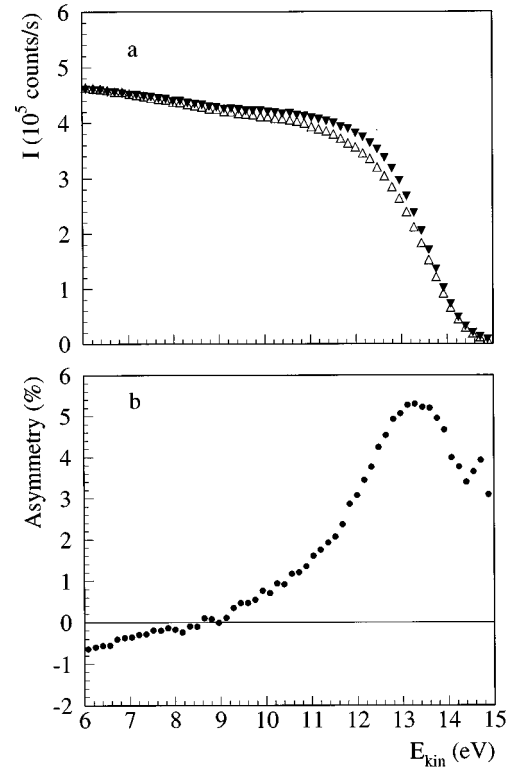


FIG. 1. (a) Energy distribution curves of electrons produced in the deexcitation of $He^*_\uparrow$ (upward pointing triangles) and of $He^*_\downarrow$ (downward pointing triangles). (b) Asymmetry function calculated from the spectra of (a) [Eq. (1.1); $P = 84\%$].

which, according to the theory of Ref. 9, indicates a predominance of minority spin states.

Finally we observe some differences in the behaviour of $A^{expt}(E)$ with respect to our previous SPMDS data on the same system[17] and to SPMDS data on Fe/W(110) (Ref. 14) and on Fe/GaAs.[15] In particular, here we do not observe a positive structure at 6–7 eV (kinetic energy) which was detected there. We were able to eliminate this feature by lowering the temperature of the substrate and reducing the emission of CO during deposition. That feature in fact is due to the spin polarization of $O_{2p}$ states derived from CO dissociation. This conclusion is supported by a study of oxygen absorption on the film as a function of exposure which will be presented elsewhere,[19] and a preliminary analysis of CO absorption as function of exposure and temperature.

## IV. RESULTS

The model introduced in Sec. II will now be discussed by comparing its results with the experimental data of Fig. 1. The $\rho_\uparrow(E)$ and $\rho_\downarrow(E)$ densities build with the superposition of Gaussian functions varying the parameters (energy position, width, and intensity), until a good agreement between calculated and experimental quantities is obtained.

In principle then we have two unknown functions ($\rho_{\uparrow(\downarrow)}(E)$) to be determined from the fit of two experimental functions ($A^{expt}(E)$ and $I^{expt}(E)$). In practice, however, $I^{expt}(E)$ cannot be directly compared with $N(E)$ essentially for two reasons: the transmission function of the electron energy analyzer is not accurately known, and the background

in the spectrum generated by secondary electrons cannot be determined precisely.

For these reasons the comparison between $I^{expt}(E)$ and $N(E)$ is made after normalization of the two functions to the maximum. In this way, we are able to define the relative weight of the structures which are present in the effective charge $(\rho_\uparrow + \rho_\downarrow)$ and magnetization $(\rho_\uparrow - \rho_\downarrow)$ densities, but not their absolute values.

A further point to be addressed concerns the definition of the onset at high kinetic energies of the experimental spectrum $(E_{max})$. The experimental EDC presents a broad onset because of the uncertainty of the neutralization distance which causes an uncertainty of $E_{1s}(z)$, the ionization potential of He$^+$. In our model, instead, $z_n$ and $E_{1s}(z_n)$ are fixed so that the onset of $N(E)$ will occur at a well-defined energy. The model then cannot reproduce the onset of the spectrum, and the influence of the choice of $E_{max}$ on calculations has to be checked carefully.

In Fig. 2 we show the comparison between $N(E)$ and $I^{expt}(E)$ [Fig. 2(a)], and between $A(E)$ and $A^{expt}(E)$ [Fig. 2(b)]. $N(E)$ and $A(E)$ are calculated starting from the functions $\rho_{\uparrow(\downarrow)}(E)$ that produce the effective charge density $n(E)$ and the effective magnetization density $m(E)$ reported in Figs. 2(c) and 2(d), respectively. In Fig. 2(c) the $\rho_\uparrow$ and $\rho_\downarrow$ components are reported as thin and dash-dotted lines, respectively. Here, as in the figures which follow, the experimental data are represented by dots, and calculated functions by lines. We observe that the experimental data are reproduced with high accuracy. As expected, a discrepancy is detected in Fig. 2(a) near $E_{max}$, as the model cannot reproduce correctly the behaviour of the spectrum in that region of energies.

If we shift the origin of the spectrum (position of $E_{max}$), we observe that the quality of the fit remains essentially unchanged with only a small influence on $n(E)$ and $m(E)$. We can conclude then that the uncertainty on $E_{max}$ reflects in the position of the energy scale but does not introduce significant distortions of the features in $n(E)$ and $m(E)$. This check was performed by shifting $E_{max}$ in an energy range 400 meV wide, sufficient to account for the uncertainty of the onset of the EDC [See Fig. 1(a)].

We now investigate the sensitivity of the model to the variations of $n(E)$ and $m(E)$. First we modify $\rho_{\uparrow(\downarrow)}(E)$ in order to change $m(E)$ with respect to $m(E)$ of Fig. 2, while leaving $n(E)$ practically unchanged. The results are reported in Fig. 3 together with the calculated functions of Fig. 2 (dash-dotted lines) which provide the best fit to the experimental data. We observe that a small variation of $m(E)$ in the region around 4.5 eV induces a significant change of $A(E)$ [Fig. 3(b)], well outside the experimental uncertainty, with minor effects on $N(E)$ [Fig. 3(a)].

The functions $\rho_{\uparrow(\downarrow)}(E)$ were then chosen in order to modify $n(E)$ while leaving $m(E)$ practically unchanged [always with respect to Figs. 2(c) and 2(d)]. The results are shown in Fig. 4, and demonstrate that, while the asymmetry shows only minor changes [Fig. 4(b)], $N(E)$ is strongly modified and does not reproduce the experimental data anymore [Fig. 4(a)]. Again, the calculated functions of Figs. 2(c) and 2(d) are reported as dash-dotted lines.

Figures 3 and 4 show that $N(E)$ is determined only by the shape of $n(E)$, as expected by its definition [denominator of
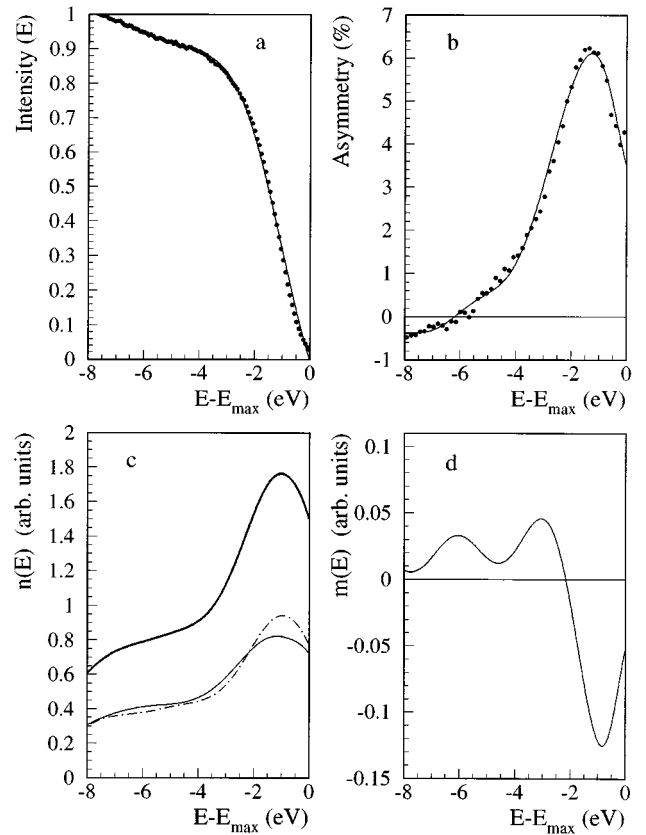


FIG. 2. (a) Comparison between calculated $N(E)$ (continuous line) and $I^{expt}(E)$, the EDC measured with unpolarized He* (dots). (b) Comparison between experimental (dots) and calculated [Eq. (2.24), line] asymmetry. (c) Effective charge density $[\rho_\uparrow(E) + \rho_\downarrow(E)$; thick line]. Majority $[\rho_\uparrow(E)$, thin line] and minority $[\rho_\downarrow(E)$, dash-dotted line] components are also shown. (d) Effective magnetization density $m(E) = \rho_\uparrow(E) - \rho_\downarrow(E)$.

Eq. (2.24)], and that $A(E)$ instead is sensitive to $m(E)$ but also depends, even if to a much lower extent, on $n(E)$. The influence of the presence of secondary electrons on $n(E)$ and $m(E)$ was also tested by subtracting a *reasonable*, exponential background from the measured EDC's (the same from both $I_\uparrow^{expt}$ and $I_\downarrow^{expt}$). This correction obviously also affects the intensity of $A^{expt}(E)$ at low kinetic energies, but modifies only slightly the intensities of $n(E)$ and $m(E)$ without any influence on the energy position of their structures.

We may then conclude that $I^{expt}(E)$ and $A^{expt}(E)$ can be reproduced only if $\rho_{\uparrow(\downarrow)}(E)$ are chosen with high accuracy, as we observe that the calculations are very sensitive to the shape of $\rho_{\uparrow(\downarrow)}$. In particular, we have seen that minor changes in $m(E)$ have a strong influence on $A(E)$.

## V. DISCUSSION

In this section we will discuss the structures which are present in $n(E)$ and $m(E)$ in order to determine their physical significance. This task will be performed by a comparison with available experimental and theoretical data on the same or related systems.

We start the discussion by considering the effective density of states $n(E)$ reported in Fig. 2(c). We observe an intense feature near $E_{max}$ with a smaller contribution toward
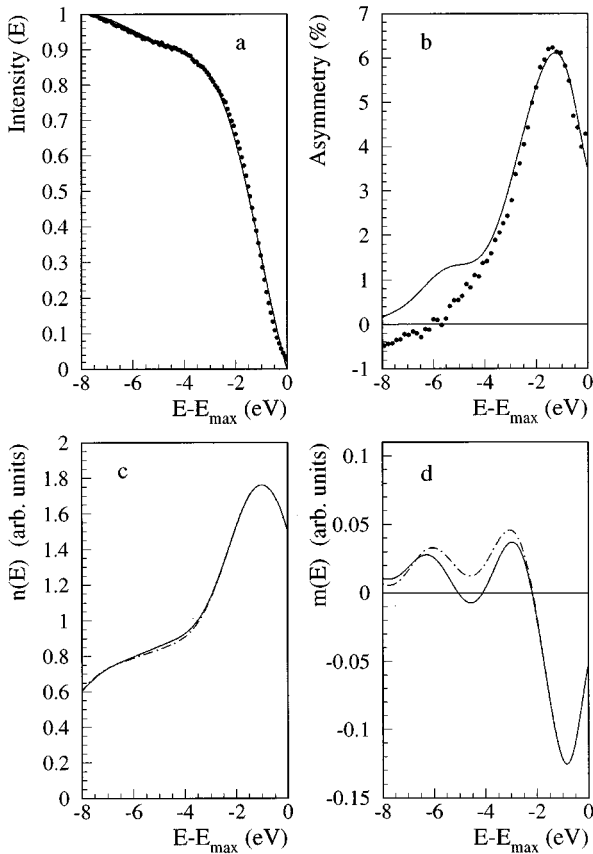
FIG. 3. Effect on $N(E)$ and $A(E)$ of a variation of $m(E)$ with respect to the reference function of Fig. 2(d). $n(E)$ and $m(E)$ of Figs. 2(c) and 2(d) are reported as dash-dotted lines.
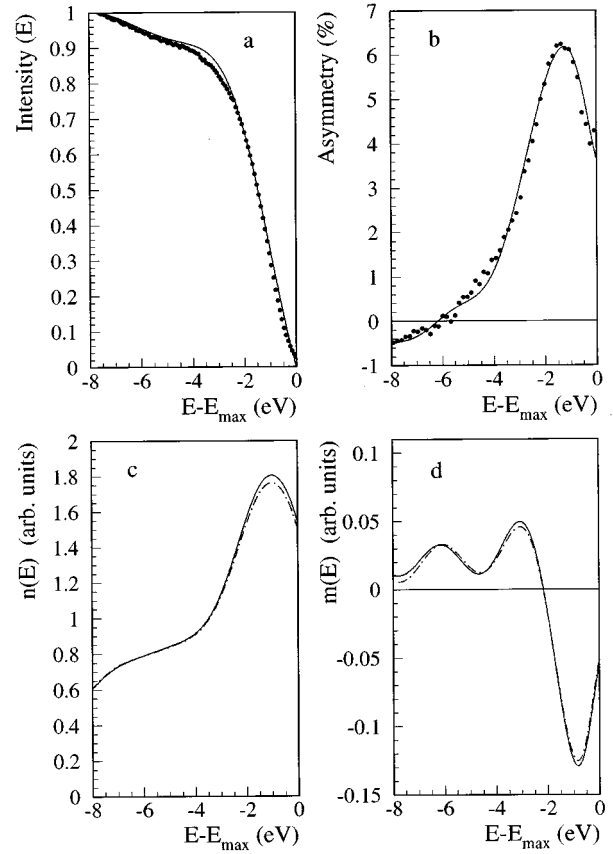


FIG. 4. Effect on $N(E)$ and $A(E)$ of a variation of $n(E)$ with respect to the reference function of Fig. 2(c). $n(E)$ and $m(E)$ of Figs. 2(c) and 2(d) are reported as dash-dotted lines.

higher binding energies. Qualitatively this is consistent with the calculated density of states of iron,[20] which presents strong contributions of $d$ states in the 0-3-eV (binding energy) region.

Concerning the majority (minority) composition of $n(E)$, we observe that their maxima are separated by $\simeq 0.3$ eV [see Fig. 2(c)]. Experimental data from spin-resolved photoemission on a Fe(100) single crystal by Brookes, Chang, and Johnson,[21] and on an Fe film grown at room temperature on a Ag(100) substrate by Jonker et al.,[22] show a majority peak at 0.6–0.7 eV (binding energy) and a stronger minority peak at 0.3 eV (binding energy). The difference in energy of these peaks compares extremely well with the energy separation of the maxima of $\rho_\uparrow$ and $\rho_\downarrow$ in Fig. 2(c).

The unbalance of $\rho_{\uparrow(\downarrow)}$ near $E_{max}$ produces the deep minimum of $m(E)$ at $E-E_{max} \simeq 0.8$ eV [see Fig. 2(d)]. Moving from this minimum toward higher binding energies, we detect a first maximum in $m(E)$ at $E-E_{max} \simeq 3$ eV. This structure compares quite well with a maximum in the majority EDC detected in spin-resolved photoemission[21,22] at 2.5 eV (binding energy) with $s$-polarized light.

A second maximum of $m(E)$ is detected at $E-E_{max} \simeq 6$ eV, in a region where spin-resolved photoemission data do not report any structure. Calculated spin-resolved density of states[20] provide $s$-$p$ contributions in this region of energies. Furthermore, at these energies, calculations show that the density of $d$ states practically vanishes in its minority component, while is still present in its majority component.

The first conclusion we can draw is then that all the features present in $n(E)$ and $m(E)$ are consistent with the available experimental and theoretical data. While the energy differences between the structures which are present in $m(E)$ and $n(E)$ are in good agreement with previous data, their absolute positions seem to be shifted toward higher binding energies by $\simeq 0.5$ eV. This shift could be partially accounted for by the indetermination we have in the choice of $E_{max}$, as discussed previously.

We also notice that SPMDS data on Fe/W(110) (Ref. 14) and Fe/GaAs (Ref. 15) show a maximum of the asymmetry right at the onset of the spectrum, while, here, the maximum of $A^{expt}(E)$ is located well inside the rising part of the EDC. We can speculate that this behaviour could be related to the surface disorder of the Fe/Ag film which could quench the asymmetry near $E_F$. This would result in a reduction of the intensity of $A^{expt}(E)$ as discussed in Sec. III, and in an energy shift toward higher binding energies. The study of the surface of an Fe(100) single crystal should clarify this hypothesis.

Finally we will discuss the relative intensities of the features which are present in $m(E)$. We observe that the negative component of $m(E)$ is definitively larger than the positive ones. This observation is consistent with previous SPMDS data on several systems,[7,9,14,15] where the detection of a positive asymmetry was interpreted in terms of a negative magnetization.

To understand this finding we must recall that we are dealing with an effective magnetization density, i.e., the true magnetization density weighted by the matrix elements which enter into the neutralization of He$^+$. As discussed in Sec. I, we may expect that $s$-$p$ states, which extend into vacuum more than $d$ states, contribute more effectively to the process. This means that the features of $n(E)$ and $m(E)$ should be dominated by the density of $s$-$p$ states, though $d$ contributions are also detected. A disentangling of $s$-$p$ and $d$ contributions in the He$^*$ data could only be provided by an accurate evaluation of the matrix elements which enter in the neutralization process.

## VI. CONCLUSIONS

Starting from the theoretical model proposed by Penn and Apell[9] to interpret SPMDS data on a magnetic surface, we developed a simple model which provides quantitative information on the surface density of states and the surface magnetization. The model is based on the simplifying assumption that the He$^+_{\uparrow(\downarrow)}$ ion which is formed after the first step of the (RI+AN) deexcitation process of He$^*_{\uparrow(\downarrow)}$ will be neutralized at a well defined distance from the surface which is independent on the spin polarization. This assumption, which could appear exceedingly crude, proves to be quite reasonable as it is able to provide meaningful results.

The model, in fact, has been tested on a case system: a 10-ML Fe film grown at $T = 120$ K on Ag(100). The test has demonstrated that from the experimental data [both the energy distribution curve of the ejected electrons $I^{\text{expt}}(E)$ and the asymmetry $A^{\text{expt}}(E)$], it is possible to derive the effective density of states $n(E)$ and the effective magnetization $m(E)$. Although we calculate effective charge and magnetization densities weighted by the matrix elements entering into the neutralization process, the comparison with

theoretical[20] and experimental data[21,22] on the same system has shown that the relevant features are well reproduced. The fine details of $n(E)$ and $m(E)$ are then not numerical artifacts necessary to reproduce the data, but have a physical significance. In particular, the shift in energy between the majority and minority states detected near the Fermi edge by spin-polarized photoemission data,[21,22] is well reproduced by the effective, spin-selected densities $\rho_{\uparrow(\downarrow)}(E)$. This agreement does not seem to be limited to the Fe/Ag case.

Currently, the model is applied to the study of oxygen chemisorption on the surface of the Fe/Ag film and, also for this system, is able to provide the relevant features of $n(E)$ and $m(E)$. In particular, it is able to reproduce the exchange split of $O_{2p}$ states which have been detected on the Fe(100)$-p(1\times1)O$ phase by spin-polarized photoemission data.[23]

The single neutralization distance model, has then proved to be not an unreasonable assumption, and work is in progress to introduce spin-dependent neutralization distances. From the results reported here we will not expect significant changes of $n(E)$ and $m(E)$ with respect to the single distance version of the model; the major differences are expected to occur near $E_{\text{max}}$, as the spin-dependent neutralization distances should introduce a broadening of $N(E)$ in that region of energies where, now, we observe the major discrepancies with the experimental data.

We can conclude that the simplicity and effectiveness of the model allow us to foresee that SPMDS data could be easily employed to extract meaningful information about surface magnetism. This will allow us to exploit fully the surface sensitivity of this experimental technique in order to obtain not only qualitative but also quantitative information which should be particularly valuable in the case of thin films at the monolayer level, and to study the influence of adsorbates on magnetic properties.

*Present address: MPI fur Mikrostrukturphysik, Weinberg 2, D-06120 Halle, Germany.

†Corresponding author. Electronic address: Mattera@ge.infn.it

[1] *Ultrathin Magnetic Structures*, edited by B. Heirich and J. A. C. Bland (Springer-Verlag, Berlin, 1994), Vols. I and II.

[2] T. Shinjo, Surf. Sci. Rep. **12**, 49 (1991).

[3] M. Wuttig, B. Feldmann, and T. Flores, Surf. Sci. **331-333**, 659 (1995).

[4] N. C. Koon, B. T. Jonker, F. A. Volkening, J. J. Krebs, and G. A. Prinz, Phys. Rev. Lett. **59**, 2463 (1987).

[5] B. Heinrich and J. F. Cochran, Adv. Phys. **42**, 523 (1993).

[6] F. B. Dunning, C. Rau, and G. K. Walters, Comments Solid State Phys. **12**, 17 (1986).

[7] M. Onellion, M. W. Hart, F. B. Dunning, and G. K. Walters, Phys. Rev. Lett. **52**, 380 (1984).

[8] H. Hagstrum, Phys. Rev. **96**, 336 (1954); **139A**, 526 (1965); **150**, 495 (1966).

[9] D. Penn and P. Apell, Phys. Rev. B **41**, 3303 (1990).

[10] W. Sesselmann, B. Woratschek, J. Kuppers, G. Ertl, and H. Haberland, Phys. Rev. B **35**, 1547 (1987).

[11] M. Salvietti, B. Granitza, A. Campora, S. Terreni, M. Canepa, and L. Mattera (unpublished).

[12] B. Granitza, M. Salvietti, E. Torello, A. Sasso, and L. Mattera, Rev. Sci. Instrum. **66**, 4170 (1995).

[13] G. Panaccione, G. Stefani, S. Terreni, L. Mattera, S. Iacobucci, M. Salvietti, G. Paolicelli, and M. Sacchi, Rev. Sci. Instrum. (to be published).

[14] G. Baum, D. Egert, M. Getzlaff, W. Raith, and H. Steidl, J. Magn. Magn. Mater. **148**, 179 (1995).

[15] M. S. Hammond, F. B. Dunning, G. K. Walters, and G. A. Prinz, Phys. Rev. B **45**, 3674 (1992).

[16] M. Canepa, M. Salvietti, Andrea Campora, and L. Mattera, J. Electron. Spectrosc. Relat. Phenom. **76**, 471 (1995).

[17] M. Salvietti, R. Moroni, M. Canepa, and L. Mattera, J. Electron. Spectrosc. Relat. Phenom. **76**, 677 (1995).

[18] M. Canepa, E. Magnano, Andrea Campora, P. Cantini, M. Salvietti, and L. Mattera, Surf. Sci. **352-354**, 36 (1996).

[19] M. Salvietti, P. Ferro, R. Moroni, M. Canepa, and L. Mattera, Surf. Sci. (to be published).

[20] S. Ohnishi, A. J. Freeman, and M. Weinert, Phys. Rev. B **28**, 6741 (1983).

[21] N. Brookes, Y. Chang, and P. D. Johnson, Phys. Rev. B **50**, 15 330 (1994).

[22] B. T. Jonker, K.-H. Walker, E. Kisker, G. A. Prinz, and C. Carbone, Phys. Rev. Lett. **57**, 142 (1986).

[23] A. Clarke, N. B. Brookes, P. D. Johnson, M. Weinert, B. Sinkovic, and N. V. Smith, Phys. Rev. B **41**, 9659 (1990).